Transient dynamics in drop impact on a superheated surface

Sang-Hyeon Lee, Sang Jun Lee, Ji San Lee, Kamel Fezzaa, and Jung Ho Je

Phys. Rev. Fluids **3**, 124308 — Published 26 December 2018

DOI: 10.1103/PhysRevFluids.3.124308

Transient dynamics in drop impact on a superheated surface

Sang-Hyeon Lee[1], **Sang Jun Lee**[1], **Ji San Lee**[1], **Kamel Fezzaa**[2], **and Jung Ho Je**[1,†]

[1]*X-ray Imaging Center, Department of Materials Science and Engineering, Pohang University of Science and Technology, 77 Cheongam-Ro, Nam-Gu, Pohang, 37673, Korea.*

[2]*X-ray Science Division, Advanced Photon Source, Argonne National Laboratory, 9700 South Cass Avenue Argonne Illinois 60439, USA.*

E-mail: [†]jhje@postech.ac.kr

PACS numbers : 68.08.Bc, 44.35.+c, 68.37.Yz

Abstract

When a drop impinges on a superheated surface, a *Leidenfrost* vapor layer forms between the drop and the surface. Transient dynamics of the layer can play a critical role for cooling in power plants but is not fully understood. Here we successfully visualize transient dynamics of the layer using ultrafast X-ray imaging. We reveal that a vapor disk with a homogeneous thickness, developed during drop impact, grows in thickness following the Fourier law. At a certain thickness (12 ± 2 μm in this study) of the vapor disk, ripples generate at its periphery due to capillary waves, resulting in significant enhancement of drop vaporization.

Ⅰ. Introduction

When a liquid drop falls on a very hot cooking pan, drop dancing is frequently observed on the pan instead of rapid vaporization. The impinging drop on a surface significantly hotter than the liquid boiling point produces an insulating vapor layer toward the surface, which keeps the liquid drop from boiling quickly and bounces it back, known as 'dynamic Leidenfrost phenomenon' [1-3]. This phenomenon is a bottle neck for spray cooling in power plants [3] or fuel evaporation in combustion engines [4,5]. However, the transient dynamics of the vapor layer before the drop bounces back, which plays an essential role in effective heat transfer, has been largely unexplored [6-14] mostly due to lack of appropriate visualization methods, despite the observation of the dynamic Leidenfrost phenomenon more than two hundred years ago [1-3].

To study transient dynamics of the dynamic Leidenfrost phenomenon, it is necessary to visualize in *real time* the interface profiles between the liquid drop and the vapor layer. This is however a challenging task with conventional optical imaging because of substantial refraction and scattering of visible light [12,15,16]. Interferometry or total internal-reflection microscopy, although recently being tried [8,11,14], is not appropriate to track the steep and complex profiles of the liquid-vapor (L-V) interface.

For transient dynamics of the Leidenfrost phenomenon in drop impact, we adopt ultrafast X-ray imaging that allows to directly visualize the L-V interface profiles in *real-time*. We reveal that a vapor disk with a homogeneous thickness, developed during drop impact, grows in thickness following the Fourier law. At a certain thickness of the vapor disk, ripples are generated at its periphery due to capillary waves, and their amplitude rapidly increases while they propagate to the center. Interestingly, rippling enhances drop vaporization rate significantly.

Ⅱ. Experiments

To clearly visualize transient dynamics of a Leidenfrost vapor layer during drop impact, we utilize ultrafast X-ray imaging coupled with a drop impact set-up [17-20] , which allows in-line projection imaging of both the drop liquid phase and the vapor layer, as schematically illustrated in Fig. 1(a). Refraction and scattering, which are substantial in optical imaging [15,16], are negligible in 'phase contrast X-ray imaging' as employed here, permitting to very clearly visualize internal boundaries in fluids [17-20]. The edge-enhanced phase contrast imaging [17] with μs time resolution provides unprecedented visualization of the transient dynamics in drop impact on a heated substrate, as demonstrated in representative snapshot images of Fig. 1(b), taken for an ethanol drop at T_s (substrate temperature) = 590 ˚C ($\gg$ T_L (Leidenfrost temperature) of ethanol, ~ 200 ˚C [8]) (see Movie 1 [21]).

Ultrafast X-ray imaging in this study was conducted at the 32-ID undulator beamline of the Advanced Photon Source, Argonne National Laboratory, to achieve the high spatial and temporal resolution required for this experiment from bright white X-ray beam (~ 10^{14} ph/s/mm^2/0.1%bw). The imaging system consists of a fast scintillator (LuAG:Ce, decay time ~ 50 ns) and a mirror coupled to a high-speed camera (Photron Fastcam SA 1.1) via a microscope objective lens (10x with NA=0.21). The detector system is synchronized to the X-ray pulses to enable direct visualization of the transient dynamics with the high spatial (~ 2 μm) and temporal (~ 3.68 μs) resolutions, with a 472 ns exposure time for each frame, which are suited for understanding transient dynamics of the vapor layers. The hard X-ray irradiation does not significantly affect the properties of liquids in very short exposures (< 300 μs) [22].

We employed ethanol, isopropanol, and methanol for liquid drops, mostly due to their low latent heats (L = 664 ~ 1103 J/g), which facilitate sufficiently thick vapor layers to be easily captured with X-ray imaging in real-time. Liquid drops were dispensed from a 27G syringe needle (outer diameter ~ 0.46mm, inner diameter ~ 0.25 mm) at heights from 3.3 to 8 cm (Weber number (= $\rho D U_0^2/\sigma$) = 55 ~ 130, ρ_l is the liquid density, D is the diameter of the liquid drop, U_0 is the impact velocity, and σ is the surface tension of the liquid). The range of the Weber numbers is appropriate to demonstrate the dynamic Leidenfrost phenomenon because liquid drops are broken as called drop atomization at the Weber numbers higher than 150. A laser triggering system was installed to sense the falling drop and to trigger the camera and the fast shutter to take the images [17-20]. Si wafer (1mm thick) was used as a substrate and heated by a substrate heater (SU-200-IH, Maivac). The substrate temperature (T_s) was measured by a thermocouple (UNI-T UT325) and controlled within 1% temperature variation from 320 ˚C to 590 ˚C, as corresponded with the film boiling regime (T_s > 200˚C) [8]. Cooling effect of substrate during the drop impact is negligible because the thermal time scale ($\tau_{th} = k_s \rho_s C_p h^{-2}$ ≅ 10^{-2} s ,where k_s is the thermal conductivity of the substrate, ρ_s is the substrate density, C_p is the specific heat of the substrate, and h is the heat transfer coefficient from the substrate to the drop) is much larger than the impact time scale (D/U_0 ≅ 10^{-4}s) [8]. The physical properties of the liquid are not much dependent on the substrate temperature in the film boiling regime since the temperature of the liquid, in particular, near the liquid-vapor interface is usually considered constant as the boiling point of the liquid [2].

As demonstrated in Fig. 1(b), taken from the blue dashed box region of Fig. 1(a), a vapor disk with roughly a homogeneous thickness (yellow dashed box in Fig. 1(b)) is developed between a liquid layer (white arrow) and the substrate at $t = 0.43$ ms during drop impact. Here the time at the impact moment is set to $t = 0$. The vapor disk continuously grows in thickness (from $t = 0.43$ to 1.15 ms). Then, interestingly, ripples are generated at the periphery of the disk (red arrow at $t = 1.15$ ms in Fig. 1(b)) and propagate to the center while growing in amplitude (orange arrow heads of Fig. 1(b) and Movie 1[21]), largely deviating from the well-known disk model [3]. The transient dynamics of the vapor layer is depicted schematically in Fig. 1(c), which is consistently observed at various temperatures far above T_L, as demonstrated in Fig. 2.

Ⅲ. Results and Discussion

A. Growth of the vapor disk

The continuous growth of the vapor disk in thickness (Fig. 1(b)) is observed for all temperatures tested (T_s (= 320 ˚C to 590 ˚C) $\gg$ T_L), as demonstrated in Fig. 3(a). Interestingly, we note that the thicknesses linearly increase with the square root of time until before rippling, regardless of T_s, as seen in Fig. 3(b). The thickness growth rate of a vapor disk can be expressed by the vaporization rate at the L-V interface (Q_v) minus the vapor flow rate out of the disk edge (Q_{out}) (see Fig. 3(c)) [2]. The vaporization at the interface is mostly due to heat conduction across the vapor disk because heat transfer by convection or radiation is negligible for the temperatures far below 1000 ˚C [2]. Then, Q_v can be estimated as

$$Q_v \sim \frac{k\Delta T}{L\delta} A \tag{1}$$

from the Fourier's heat conduction law, where k is the thermal conductivity of the vapor, ΔT is the temperature difference between T_s and T_b (boiling temperature of the liquid drop), A is the cross-sectional area of the vapor disk, L is the latent heat of the liquid, and δ is the vapor disk thickness.

Q_{out} can be simply represented by mass transport [13] as

$$Q_{out} \sim \rho_v D \delta U_v \tag{2}$$

where ρ_v is the vapor density and U_v is the velocity of the vapors flowing out of the disk edge. For a vapor disk with a very thin thickness compared to its diameter, U_v can be estimated using the lubrication theory [3,13]:

$$\frac{\partial P}{\partial r} \sim \mu_v \frac{\partial^2 U_v}{\partial z^2} \tag{3}$$

where r and z are the coordinates in the radial and vertical directions, respectively. P is the fluid pressure, which corresponds to the dynamic pressure ($\sim\rho_l U_0^2$) in drop impact, and μ_v is the viscosity of the vapor. By taking $\partial_r P \sim \rho_l U_0^2 / D$ and $\partial_z^2 U_v \sim U_v / \delta^2$ [13], we obtain

$$U_v \sim \frac{\rho_l U_0^2}{\mu_v D} \delta^2 \tag{4}$$

From Eqs. (2) and (4), Q_{out} is obtained as

$$Q_{out} \sim \frac{\rho_v \rho_l U_0^2}{\mu_v} \delta^3 \tag{5}$$

We calculated Q_{out} and Q_v using Eqs. (1) and (5) for three liquids (ethanol, isopropanol and methanol), as shown in Table 1. Here, the thickness of the vapor disk (δ) was taken as the largest value (12×10^{-6} m), measured after its growth till before rippling at the highest substrate temperature tested ($T_s = 590$ °C). The largest δ value corresponds to the cases of the largest Q_{out} and the smallest Q_v by Eqs. (1) and (5). It turns out that even the largest Q_{out} is two orders of magnitude smaller than the smallest Q_v for all the three liquids. Thus, Q_{out} is negligible compared to Q_v in calculating the thickness of the vapor disk. From this, the thickness of the vapor disk (δ) can be finally reduced to

$$\delta = \alpha \Delta T^{0.5} t^{0.5} \tag{6}$$

where α is a constant. Eq. (6) is well matched with the time dependence of the thickness measured for all temperatures in Fig. 3(b). This equation also explains the temperature dependence of the thickness, as plotted by $\delta/t^{0.5}$ (the slope of each curve in Fig. 3(b)) vs. $\Delta T^{0.5}$ in Fig. 3(d) . Here the constant α for ethanol is estimated as 4×10^{-5} $m/s^{0.5}/K^{0.5}$. These results indicate that the thickness growth rate of the vapor disk until before rippling is governed by the Fourier law.

B. Rippling of a vapor disk

Ripples start generating around the periphery of a vapor disk at some point (hereafter called rippling time (t_r), $t = 1.15$ ms in Fig. 1(b)) of the disk growth. After the rippling time, interestingly, the vapor thicknesses δ measured (open squares of Fig. 4(a)) become lower than those estimated by Eq. (6) (dashed line in Fig. 4(a)) and the difference gets bigger over time. It is noteworthy that the thickness δ_r (called rippling thickness) at t_r is almost invariant with ΔT, as shown in Fig. 4(b), measured as 12 ± 2 μm. In addition, the rippling time t_r is inversely proportional to ΔT, as seen in Fig. 4(c). This is consistent with the invariance of δ_r with ΔT (Fig. 4(b)), as deduced from Eq. (6) (blue dashed line in Fig. 4(c)). Here we note that δ_r is also invariant with the impact velocity of the drop (U_0) (open circles in Fig. 4(d)) while the height of the liquid layer at t_r drastically changes (open diamonds in Fig. 4(d)), indicating that the key parameter in rippling is mostly the thickness of the vapor disk, not the height of the liquid layer. These results suggest that the initiation of rippling requires the growth of the vapor disk to a certain thickness, which is 12 ± 2 μm in this case, regardless of ΔT or U_0 (Fig. 4(b) and (d)).

Rippling can be explained by capillary waves that are generated by the competition between viscosity, inertia, and surface tension for a liquid layer surrounded by another fluid [23-30]. Conceivably, a free surface is required for initiation of capillary waves [24,25,27-30]. Different from the top air-liquid *free interface* (magenta arrow head at $t = 0.77$ ms in Fig. 1(b)) of the liquid layer (white arrow in Fig. 1(b)), the bottom L-V interface (green arrow head in Fig. 1(b)) is not a free surface by the viscous force from the substrate when the vapor disk is extremely thin. This suggests that sufficient growth of the disk thickness is required for initiation of capillary waves. In fact, rippling occurs whenever the vapor disk grows to a thickness of ~12 μm ($\lesssim \delta_u$ (the boundary layer thickness (~ 36 μm)) [13, 24]), regardless of the substrate temperature (T_s : 320˚C ~ 590˚C) or impact velocity (U_0 : 0.80 m/s ~ 1.25 m/s). This indicates that rippling occurs by the initiation of capillary waves.

We note that the rippling at the L-V interface (red arrow at $t = 1.15$ ms) progresses a little later than the onset of the capillary waves on the top air-liquid interface (blue arrow at $t = 0.77$ ms) in Fig. 1(b). The delayed onsets of the capillary waves at the top and the bottom interfaces were precisely measured from the real-time X-ray snapshots for all substrate temperatures tested (Fig. 5). As ΔT increases, the time lag is getting smaller, mostly due to enhanced vaporization rate at high substrate temperatures.

Now we discuss group velocity of capillary waves that are presumably the origin of rippling. The general dispersion relation of gravity-capillary waves on the interface between two fluids is described [29] as

$$\omega^2 = (kg + k^3\sigma/\rho_l) \qquad (7)$$

where ω is the angular frequency of the wave, k (=$2\pi/\lambda$(wavelength)) is the wave number, and g is the gravitational acceleration. For very short wavelengths ($\ll$ mm) as in our drop impact cases, $k \gg \sqrt{\rho_l g/\sigma}$. Then Eq. (7) reduces to

$$\omega^2 = (k^3\sigma/\rho_l) \tag{8}$$

, which corresponds to the dispersion relation of capillary waves. The phase velocity (U_p) and the group velocity (U_g) of capillary waves can be obtained from Eq. (8) as follows.

$$U_p = \frac{\omega}{k} = \sqrt{\frac{\sigma}{\rho_l}k} \tag{9}$$

$$U_g = \frac{d\omega}{dk} = \frac{3}{2}\sqrt{\frac{\sigma}{\rho_l}k} = \frac{3}{2}\sqrt{\frac{\sigma}{\rho_l}\frac{2\pi}{\lambda}} \tag{10}$$

The capillary waves of maximal amplification have a phase velocity equal to the impact velocity of a drop, U_0 [8]; hence, Eq. (10) is reduced to

$$U_g = 1.5U_p \propto U_0 \tag{11}$$

As seen in Fig. 6(a), the velocities of ripples (red squares), directly measured from real-time X-ray snapshots, are comparable to the group velocities (blue circles) of capillary waves, calculated from Eq. (10). In Eq. (10), λ is the wavelength measured by the distance between the 1st and 2nd peaks of ripples from real-time X-ray snapshots. The measured group velocities are also linearly proportional to the impact velocity of the drop (U_0), consistent with Eq. (11). In addition, the measured group velocities are invariable to ΔT (inset of Fig. 6(a)), consistent with Eq. (10). These results confirm that the origin of rippling is capillary waves generated on the L-V interface.

The wavelength of capillary waves can be finally driven as follows from Eqs. (10) and (11).

$$\lambda \propto \frac{\sigma}{\rho_l U_0^2} \propto We^{-1} \tag{12}$$

Figure 6(b) shows that the measured wavelengths of ripples are inversely proportional to We, regardless of ΔT. This result is well matched with Eq. (12), again supporting that rippling is due to capillary waves. The low Ohnesorge numbers ($Oh = \mu/\sqrt{\rho_l \sigma D}$) of the liquid drops tested in this study ($Oh = 0.001 \sim 0.004$) are also consistent with the propagation condition of capillary waves in drop impact, Oh $\ll$ 0.01 [17, 20, 22, 25].

Here we observe similarity of wave properties (such as the group velocities or the wavelengths) between the two capillary waves along the top air-liquid and the bottom L-V interfaces, as demonstrated in Fig. 1(b) (t = 4.50 and 5.41 ms) and Movie 1 [21], and as measured for all impact velocities and temperatures tested (Table 2). This implies that the capillary waves along the bottom L-V interface be caused by the same Plateau-Rayleigh instability as in the top interface [27, 30].

C. Rippling and vaporization

Rippling significantly enhances vaporization rate of the drop. As schematically illustrated in Fig. 7(a), vapors can diffuse from the vapor disk (black arrow) into the rippling region formed by capillary waves (blue arrow). This explains that the growth rate of the disk thickness after rippling becomes lower than that estimated by the Fourier law (Eq. (6)) in Fig. 4(a). The lowering in thickness by rippling (Fig. 4(a)) can effectively lead to enhancement of the vaporization rate at the L-V interface because heat transfer across the vapor disk is inversely proportional to disk thickness.

Indeed, as shown in Fig. 7(b), the vapor volume (open circles) between the liquid layer and the substrate, measured from X-ray snapshots, is larger than that (dashed line) estimated assuming continuous growth of the vapor disk without rippling. Here, the vapor volume V between the liquid layer and the substrate was simply obtained by adding the volumes of the vapor disk (V_{disk}) and the rippling region (V_{ripple}): $V(t) = V_{disk}(t) + V_{ripple}(t)$, where $V_{\mathrm{disk}}(\mathrm{t})$ ($= \pi R(t)^2 \delta_m(t)$) and $V_{\mathrm{ripple}}(t)$ ($= 2\pi S(t) x_{cm}(t)$; Pappus's centroid theorem for solid of revolution) can be obtained by measuring $\delta_m(t)$ (the subscript m: 'measured'), $R(t)$ (the radius of the vapor disk), $S(t)$ (the cross-sectional area of the rippling region), and $x_{cm}(t)$ (the distance from the centroid to the center of mass for the rippling region) from X-ray snapshots. Meanwhile, the estimated volume of the vapor disk (dashed line in Fig. 7(b)) was simply obtained using V_{disk} ($= \pi R(t)^2 \delta(t)$), where $\delta(t)$ is calculated from Eq. (6) and $R(t)$, which has nothing to do with rippling, is taken as the measured values from X-ray snapshots. Interestingly, the enhancement of the vaporization rate by rippling in Fig. 7(b) is greater at higher substrate temperatures, which is consistent with a larger volume of the rippling region at higher temperatures (Fig. 2).

D. Growth rate of a vapor disk for different liquids

The growth rate of a vapor disk in thickness until before rippling is governed by the Fourier law (Eq. (6)) not only for ethanol but also for isopropanol and methanol, as demonstrated in the linear dependencies of δ on $t^{0.5}$ (Figs. 3(b), 8(a), and 8(b)) and of $\delta/t^{0.5}$ on $\Delta T^{0.5}$ (Fig. 8(c)). The constant α in Eq. (6) can be expressed as $\alpha = (k_v/L\rho_v)^{0.5}$, where k_v is the thermal conductivity of the vapor and ρ_v is the vapor density [2]. Here the k_v value is similar for the three liquids [31-33]. ρ_v is functions of temperature and pressure if assuming ideal gas behavior and thus ρ_v at the liquid-vapor interface is not much different for the three liquids, as seen by not much different boiling points ($T_{b\ \mathrm{ethanol}} = 351K$, $T_{b\ \mathrm{methanol}} = 338K$, and $T_{b\ \mathrm{isopropanol}} = 355K$) and by almost the same vapor pressure corresponding to the dynamic pressure ($\sim\rho_l U_0^2$) [2,12,13]. Then, α is mostly dependent on the latent heat L for the three alcohols, as demonstrated in Fig. 8(d). The solid line is the best fit with allometric scaling for the three liquids and α can be expressed as a function of L

$$\alpha\,(L) = 730 \times L^{-0.42} \tag{13}$$

in good agreement with $\alpha \sim L^{-0.5}$. Eq. (13) allows one to estimate the thickness of a vapor disk for liquids with k_v and T_b values similar to the three alcohols at arbitrary t and T_s. For instance, the vapor disk thickness for water drop (L = 2260 J/g) with k = 0.0271 W/m/K and $T_b = 373K$ is estimated as 6 μm at t = 0.3 ms and T_s = 350 ˚C using Eqs. (6) and (13), which is comparable with the vapor thickness 3 μm, measured by interferometry for the same condition [12].

Ⅳ. Conclusion

We have experimentally revealed transient dynamics of a Leidenfrost vapor layer in drop impact that is unresolvable with optical imaging. Using ultrafast X-ray imaging, we elucidate that a vapor disk with a homogeneous thickness, developed during drop impact, grows in thickness following the Fourier law. Notably, rippling occurs, due to capillary waves, at the periphery of the vapor disk at a certain thickness of the disk (12 ± 2 μm in ethanol drop) and ripples are rapidly increased in amplitude while propagated to the center. Rippling significantly enhances vaporization of liquid drop by effectively reducing the growth rate of the vapor disk thickness. The transient dynamics can offer substantial insight for further analytical, numerical and experimental work on the Leidenfrost phenomenon, which can be greatly helpful for many industrial applications such as fuel combustion or spray cooling.

Reference

[1] J.G. Leidenfrost, *De Aquae Communis Nonnullis Qualiatibus Tractatus* (Hermannus Ovenius, Duisburg, 1756).

[2] David Quéré, Leidenfrost Dynamics, Annual Review of Fluid Mechanics **45**, 197-215 (2013).

[3] M. Rein, *Drop-surface Interaction*, Springer Verlag Wien. 428 (2002).

[4] A. L. N. Moreira, A. S. Moita, and M. R. Panão, Advances and challenges in explaining fuel spray impingement: How much of single droplet impact research is useful?, Progress in Energy and Combustion Science **36**, 554-580 (2010).

[5] G. G. Wells, R. Ledesma-Aguilar, G. McHale, and K. Sefiane, A sublimation heat engine, Nat Commun **6**, 6390 (2015).

[6] L. H. J. Wachters and N. A. J Westerling, The heat transfer from a hot wall to impinging water drops in the spheroidal state, Chem. Eng. Sci. **21**, 1047-1056 (1966).

[7] I. U. Vakarelski, N. A. Patankar, J. O. Marston, D. Y. Chan and S. T. Thoroddsen, Stabilization of Leidenfrost vapour layer by textured superhydrophobic surfaces. Nature. **489**, 274-277 (2012).

[8] M. Shirota, M. A.J. van Limbeek, C. Sun, A. Prosperetti, and D. Lohse, Dynamic Leidenfrost Effect: Relevant Time and Length Scales, Phys Rev Lett **116**, 064501 (2016).

[9] B. S. Gottfried, C. J. Lee, and K. J. Bell, The Leidenfrost phenomenon:Film boiling of liquid droplets on a flat plate, Int. J. Heat Mass Transf. **9**, 1167 (1966).

[10] A. L. Biance, C. Clanet, and D. Quéré, Leidenfrost drops, Physics of Fluids. **15**, 1632 (2003).

[11] J. C. Burton, A. L. Sharpe, R. C. van der Veen, A. Franco, and S. R. Nagel, Geometry of the vapor layer under a leidenfrost drop, Phys Rev Lett **109**, 074301 (2012).

[12] T. Tran, H. J. Staat, A. Prosperetti, C. Sun, and D. Lohse, Drop impact on superheated surfaces, Phys Rev Lett **108** , 036101 (2012).

[13] T. Tran, H. J. J Staat, A. Susarrey-Arce, T. C. Foertsch, A. van Houselt, H. J. G. E. Gardeniers, A. Prosperetti, D. Lohse and C. Sun, Droplet impact on superheated micro-structured surfaces, Soft Matter **9**, 3272 (2013).

[14] M. Khavari and T. Tran, Universality of oscillating boiling in Leidenfrost transition, Phys Rev E **96**, 043102 (2017).

[15] M. M. Driscoll, C. S. Stevens, and S. R. Nagel, Thin film formation during splashing of viscous liquids, Phys. Rev.E. **82**, 036302 (2010).

[16] S. T. Thoroddsen, T. G. Etoh, K. Takehara, N. Ootsuka, and Y. Hatsuki, The air bubble entrapped under a drop impacting on a solid surface, J. Fluid Mech. **545**, 203 (2005).

[17] J. S. Lee, B. M. Weon, S. J. Park, J. H. Je, K. Fezzaa, and W. K. Lee, Size limits the formation of liquid jets during bubble bursting, Nat Commun **2**, 367 (2011).

[18] G. Agbaglah, M. J. Thoraval, S. T. Thoroddsen, L. V. Zhang, K. Fezzaa and R. D. Deegan,

Drop impact into a deep pool: vrotex shedding and jet formation, J. Fluid Mech. 764, R1 (2015).

[19] J. S. Lee, S. J. Park, J. H. Lee, B. M. Weon, K. Fezzaa, and J. H. Je, Origin and dynamics of vortex rings in drop splashing, Nat Commun **6**, 8187 (2015).

[20] J. S. Lee, B. M. Weon, J. H. Je, and K. Fezzaa, How does an air film evolve into a bubble during drop impact?, Phys Rev Lett **109** (20), 204501 (2012).

[21] Supplementary Movie

[22] B. M. Weon, J. H. Je, Y. Hwu, And G. Margaritondo, Decreased Surface Tension of Water by Hard-X-ray Irradition Phys. Rev. Lett. **100**, 217403 (2008).

[23] Museok Song and Grétar Tryggvason, The formation of thick borders on an initially stationary fluid sheet, Physics of Fluids **11**, 2487-2493 (1999).

[24] M. Pasandideh-Fard, Y. M. Qiao, S. Chandra, and J. Mostaghimi, Capillary effects during droplet impact on a solid surface, Physics of Fluids **8**, 650-659 (1996).

[25] Y. Renardy, S. Popinet, L. Duchemin, M. Renardy, S. Zaleski, C. Josserand, M. A. Drumright-Clarke, D. Richard, C. Clanet, and David Quéré, Pyramidal and toroidal water drops after impact on a solid surface, Journal of Fluid Mechanics **484**, 69-83 (2003).

[26] François Blanchette and Terry P. Bigioni, Partial coalescence of drops at liquid interfaces, Nature Physics **2** (4), 254-257 (2006).

[27] Daniel A. Weiss and Alexander L. Yarin, Single drop impact onto liquid films: neck distortion, jetting, tiny bubble entrainment, and crown formation, Journal of Fluid Mechanics **385**, 229-254 (1999);

[28] A. L. Yarin, Drop impact Dynamics: Splashing, Spreading, Receding, Bouncing..." Annual Review of Fluid Mechanics **38**, 159-192 (2006).

[29] H. Lamb. *Hydrodynamics,* 6th ed. (Cambridge University Press, Cambridge, 1932).

[30] Rayleigh, L. On the capillary Phenomena of Jets, *Proc. R. Soc.* **29**, 71-97, (1879).

[31] Hollan, P. M., Eaton, B. E., and Hanely, H. J. M., A correlation of the viscosity and thermal conductivity data of gaseous and liquid ethylene, J. Phys. Chem. Ref. Data. **12**, 917, (1983).

[32] Younglove, B. A. And Hanley, H. J. M., The viscosity and thermal conductivity coefficients of gaseous and liquid argon, *J. Phys. Chem. Ref. Data*, **15**, 1323, (1986).

[33] Kadoya, K. Matsunaga, N., and Nagashima, A.,Viscosity and Thermal Conductivity of Dry Air in the Gaseous Phase, J. Phys. Chem. Ref. Data. **14**, 947, (1985).

Acknowledgements

This research was supported by the Ministry of Trade, Industry and Energy (MOTIE) and the Korea Institute for Advancement of Technology (KIAT) through the International Cooperative R&D Program, Brain Korea 21 PLUS Project for the Center for Creative Industrial Materials and National Research Foundation of Korea(NRF) grant funded by the Korea government (2017R1E1A1A01075274). The use of the Advanced Photon Source, an Office of Science User Facility operated for the U.S. Department of Energy (DOE) Office of Science by the Argonne National Laboratory, was supported by the U.S. DOE under contract no. DE-AC02-06CH11357.

Tables

TABLE 1: Calculation of Q_{out} and Q_v for a vapor disk with a thickness δ (12 x 10^{-6} m)* and an area A (5.0 x 10^{-5} m^2)* for three different liquid drops [31-33].

	Ethanol	**Isopropanol**	**Methanol**
U_0 (m/s)	0.885		
D (m)	4.0×10^{-3}		
ΔT (K)	512	508	525
k (W/m/K)	0.0227	0.0215	0.0221
ρ_l (kg/m^3)	789	786	792
ρ_v (kg/m^3)	1.603	2.081	1.204
L (J/g)	839	664	1103
μ_v (Pa· s)	1.07×10^{-5}	0.94×10^{-5}	1.26×10^{-5}
Q_{out} (g/s)	1.7×10^{-4}	1.1×10^{-4}	2.5×10^{-4}
Q_v (g/s)	5.7×10^{-2}	6.8×10^{-2}	4.3×10^{-2}

* Here the δ value was taken as the largest thickness of a vapor disk grown just before rippling in an ethanol drop and the A value was taken at the area of the vapor disk.

TABLE 2: Group velocities (U_g) and wavelengths (λ) of the capillary waves at the top air-liquid and the bottom liquid-vapor interfaces for various substrate temperatures (T_s) and impact velocities (U_0).

(1) U_0 : 0.88 m/s

T_s (˚C)	320	370	420	460	510	550	590
U_g (Top) (m/s)	0.63±0.03	0.69±0.05	0.61±0.04	0.65±0.04	0.60±0.01	0.64±0.05	0.59±0.02
U_g (Bottom) (m/s)	0.65±0.03	0.69±0.05	0.63±0.03	0.66±0.02	0.61±0.01	0.65±0.03	0.60±0.03
λ (Top) (μm)	248±7	228±3	254±5	252±6	258±10	258±10	250±4
λ (Bottom) (μm)	254±8	249±6	253±7	248±3	255±10	243±6	248±3

(2) T_s : 420 ˚C

U_0 (m/s)	0.804	0.885	0.989	1.084	1.171	1.252
U_g (Top) (m/s)	0.58±0.03	0.61±0.04	0.65±0.02	0.70±0.04	0.79±0.02	0.82±0.02
U_g (Bottom) (m/s)	0.55±0.02	0.63±0.03	0.65±0.01	0.73±0.05	0.79±0.02	0.82±0.02
λ (Top) (μm)	382±20	253±7	226±4	172±7	146±3	134±2
λ (Bottom) (μm)	375±9	252±5	227±9	166±4	145±2	134±2

Figures

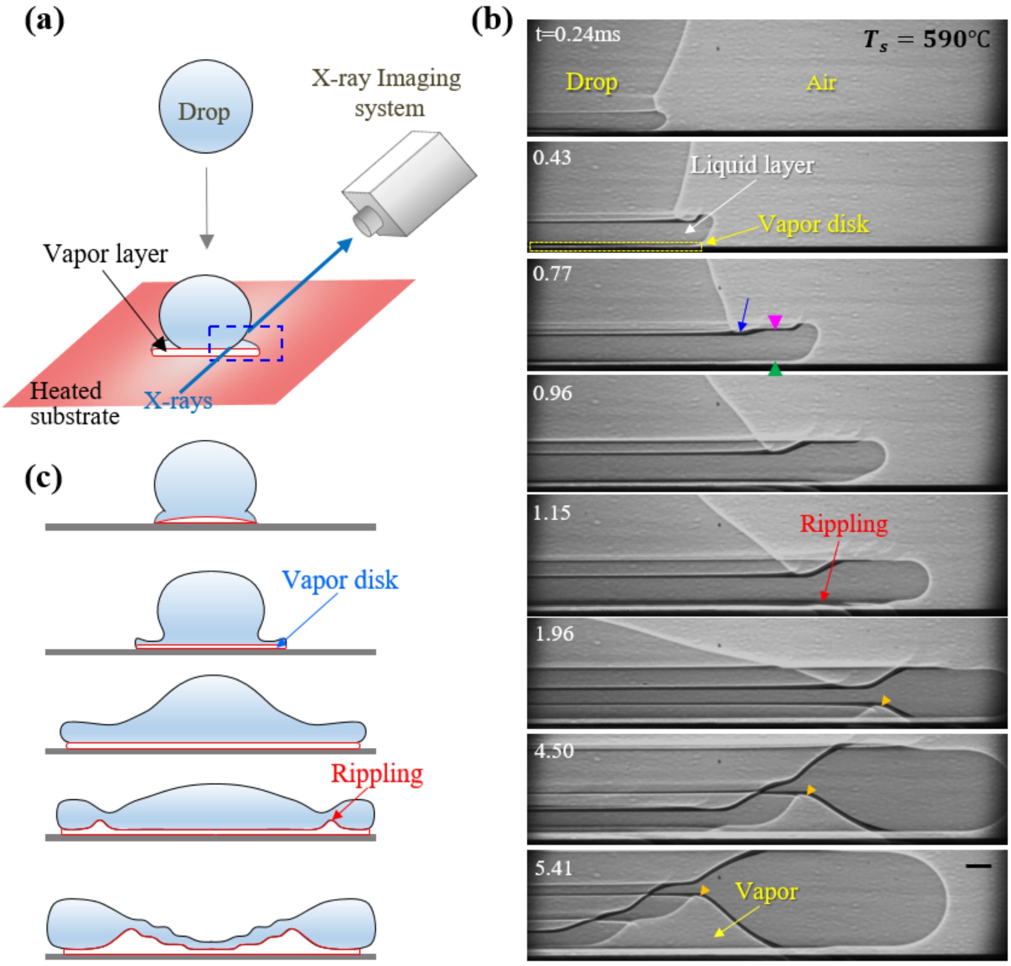

FIG. 1 (color online). Ultrafast X-ray imaging for a Leidenfrost vapor layer during drop impact. (a) Schematic of ultrafast X-ray imaging set-up for drop impact. **(b)** Sequential X-ray images, taken from the blue dashed box region of **a** in ethanol drop impact from 4cm-height on a heated substrate (T_s = 590 ˚C), showing transient dynamics of a vapor layer (Movie 1 [21]). Interfacial boundaries between the drop and the vapor layer are clearly resolved. **(c)** Illustration of the transient dynamics of the vapor layer during drop impact. Here the time at the impact moment is set to t=0. Scale bar, 100 μm long.

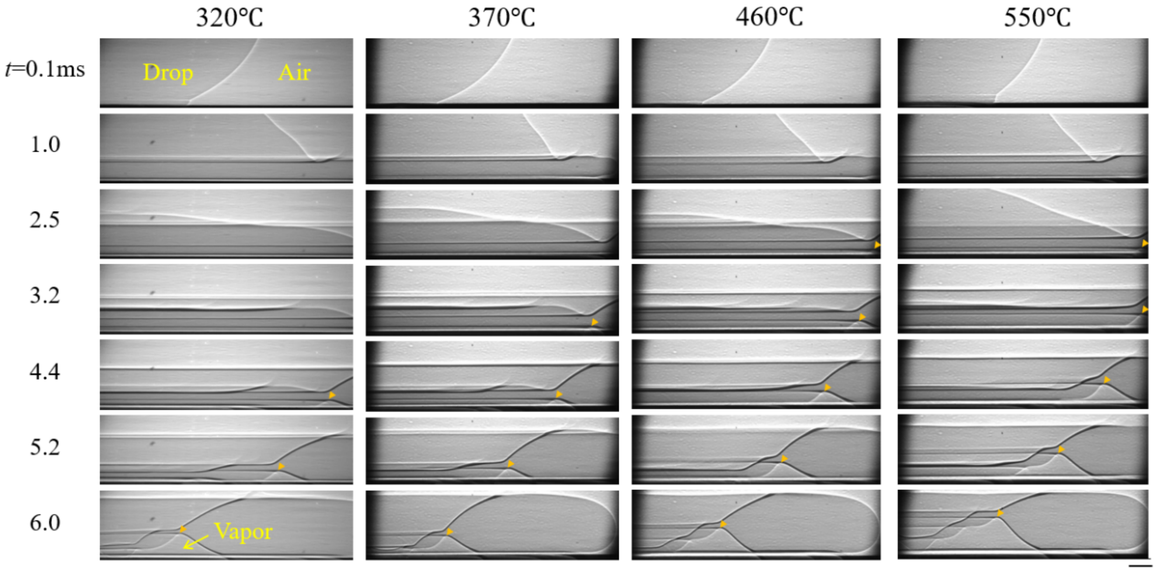

FIG. 2 Transient dynamics of the vapor layers. Representative X-ray snap-shot images for ethanol drops at 4cm-height for different substrate temperatures (T_s). Ripples are always generated and propagated to the center while growing in amplitude, as marked by orange arrow heads, for all substrate temperatures tested. Scale bar, 100 μm long.

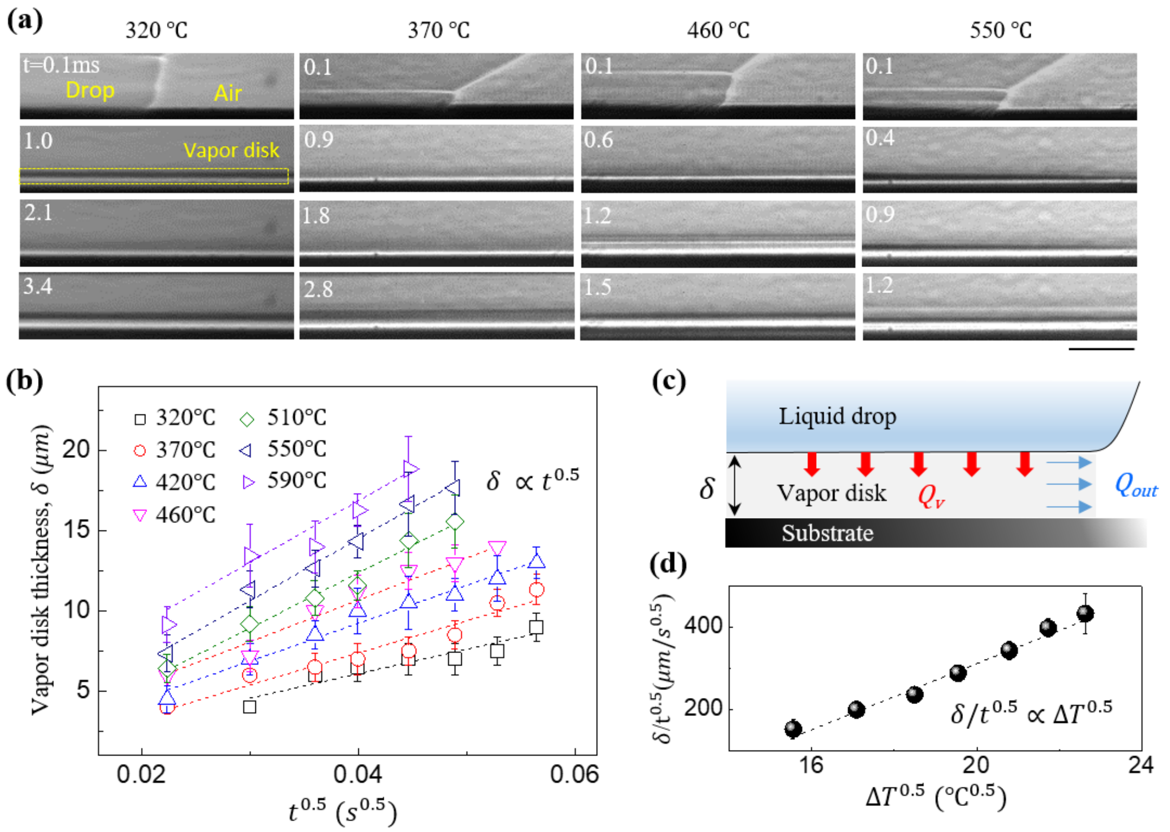

FIG. 3 (color online) Growth of the vapor disks for various substrate temperatures (T_s). **(a)** Representative X-ray snap-shot images of the vapor disks for different substrate temperatures, taken from the blue dashed box region (Fig. 1(a)) in ethanol drop impact from 4cm-height. Scale bar, 100 μm long. **(b)** Vapor disk thickness (δ) vs. $t^{0.5}$ for various substrate temperatures (T_s). The dashed lines, the best linear fitted ones, show that disk thicknesses grow with $t^{0.5}$ regardless of T_s. The error bars are s.d. from five to ten sets of the image data. **(c)** Illustration of vapor flows through a vapor disk. The thickness growth rate is determined by Q_v (vaporization rate at the liquid-vapor interface, red arrows) minus Q_{out} (vapor flow rate out of the disk edge, blue arrows). **(d)** Vapor disk thickness normalized by $t^{0.5}$ vs. $\Delta T^{0.5}$ (ΔT : the difference between T_s and T_b (the liquid boiling point)). The best fit of the slope is 4×10^{-5} $m/s^{0.5}/K^{0.5}$.

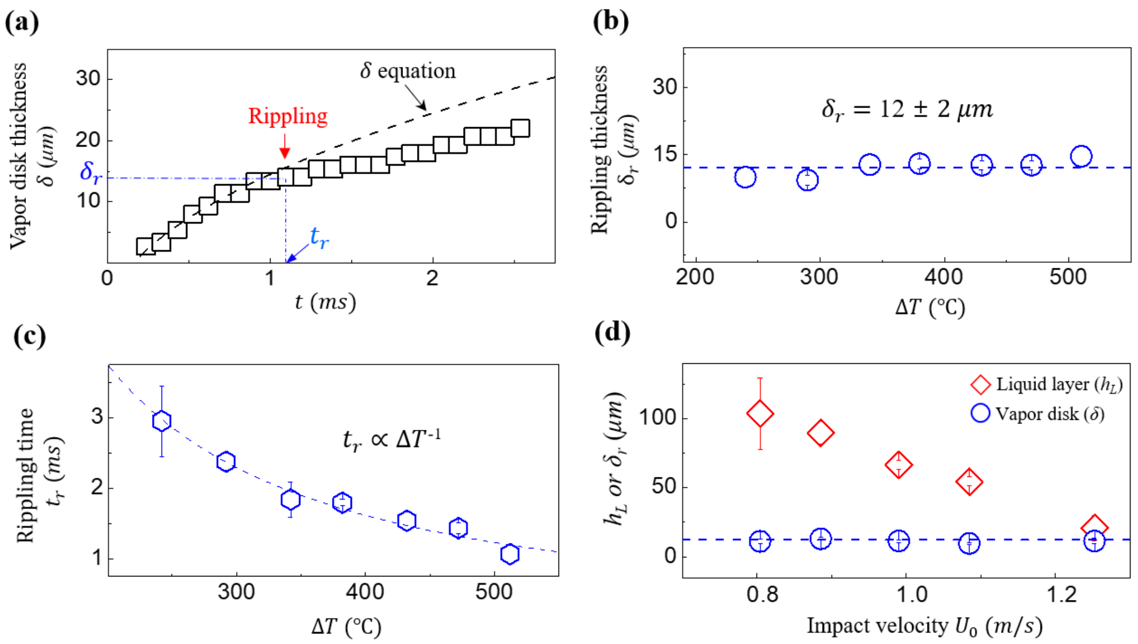

FIG. 4 (color online) Vapor disk growth in rippling (a) Vapor disk thickness vs. *t* in ethanol drop impact from 4cm-height on a heated substrate (T_s = 590 ˚C). After rippling, the disk thickness is lower than estimated (black dashed line) by the Fourier law (δ equation : Eq. (6)). **(b)** Rippling thickness (δ_r) is invariant with ΔT (=$T_s - T_b$). Dashed line represents the average value of each data, 12 ± 2 μm**. (c)** Rippling time (t_r) is inversely proportional to ΔT. **(d)** h_L (the height of the liquid layer, red diamond) and δ_r (the rippling thickness of the vapor disk, blue circle) vs. U_o (impact velocity) when the ripples are generated. δ_r is invariant with U_o while h_L drastically changes.

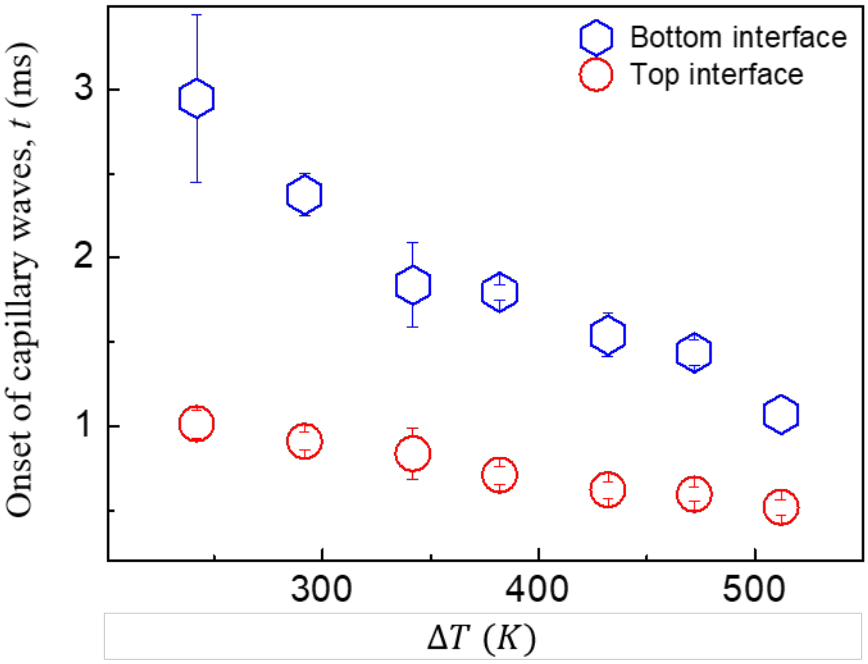

FIG. 5 (color online) Onset of capillary waves. Onsets of two types of capillary waves at the top air-liquid (red circle) and the bottom liquid-vapor (blue hexagon) interfaces as a function of ΔT (= $T_s - T_b$). The onset of capillary waves at the bottom interface is always delayed compared to that at the top interface and the time lag is getting smaller with ΔT.

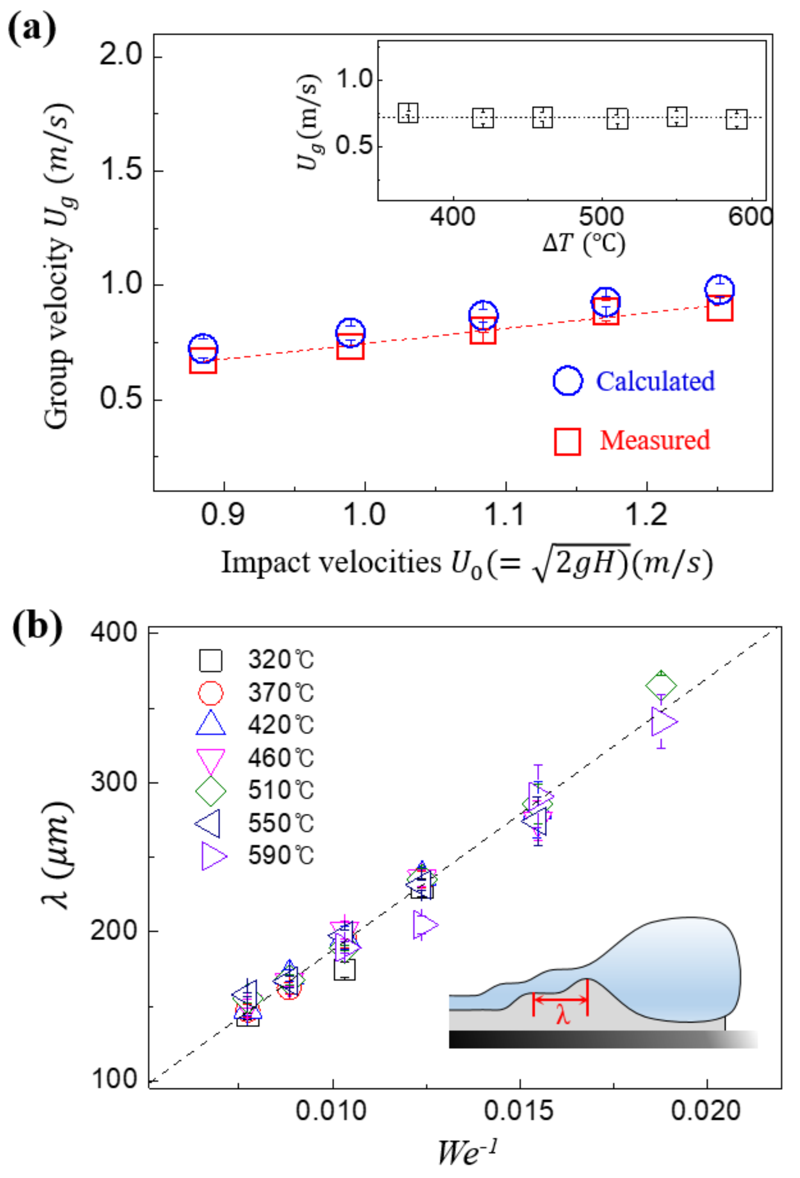

FIG. 6 (color online) Group velocity and wavelength of capillary waves. (a) Comparison of the group velocity measured (red squares) to those calculated (blue circles) assuming capillary waves in ethanol drop impact for various impact velocities ($U_0 = \sqrt{2gH}$, g is acceleration and H is the impact height). The dashed line is the linear fit of the measured data. The inset shows the group velocities measured, which are invariant with ΔT. **(b)** The wavelength of the ripples (λ), measured as the distance between their 1st and 2nd peaks, is linearly proportional to We^{-1} regardless of ΔT. The error bars are s.d. from the five to ten sets of the image data. These results suggest that the origin of the rippling is capillary waves.

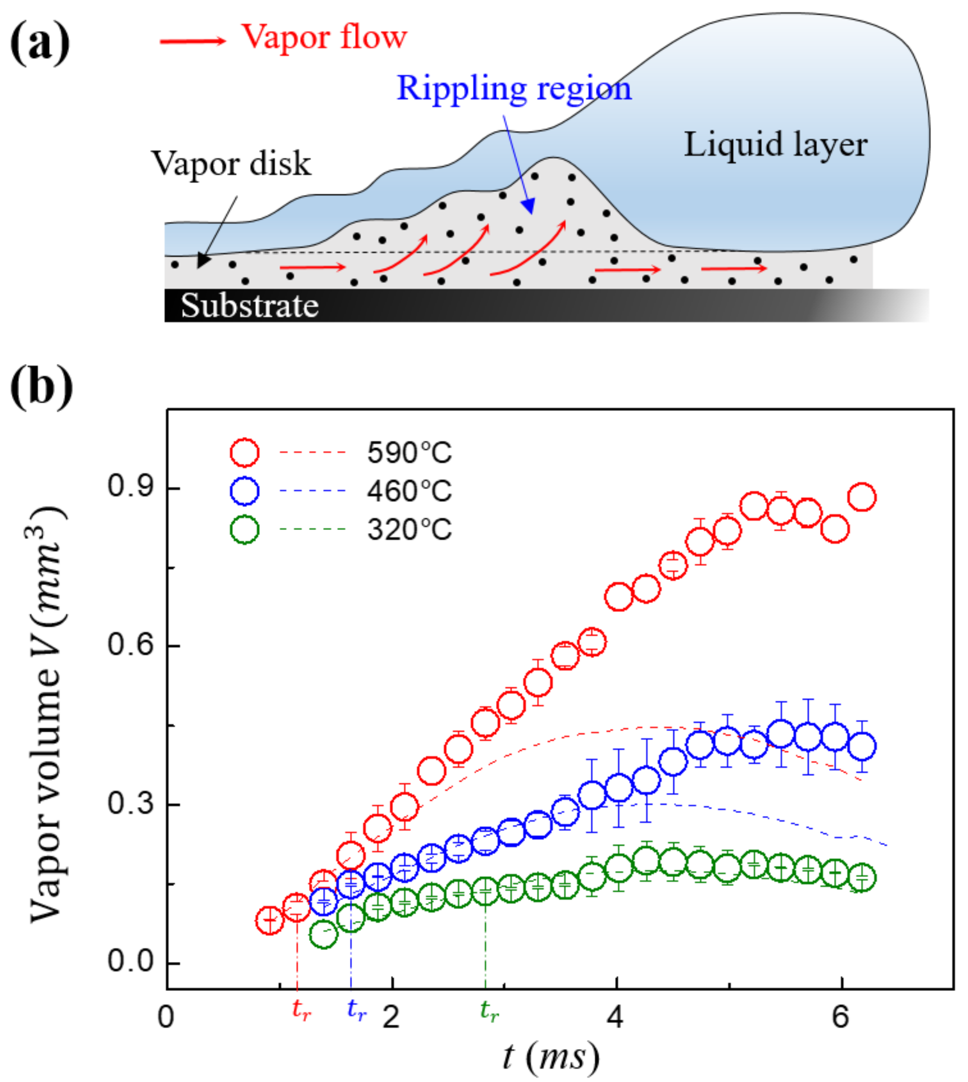

Figure 7 (color online) Enhanced vaporization by rippling. (a) Schematic of vapor diffusion from a vapor disk region into a rippling region. **(b)** V (the total vapor volume between the liquid drop and the substrate) measured (open circle) from the X-ray snapshots and estimated based on Eq. (6) (dashed line) assuming continuous growth of the vapor disk without rippling, as a function of time for different T_s. After rippling time (t_r), the measured volume is getting bigger than estimated. And the difference is getting larger at higher T_s.

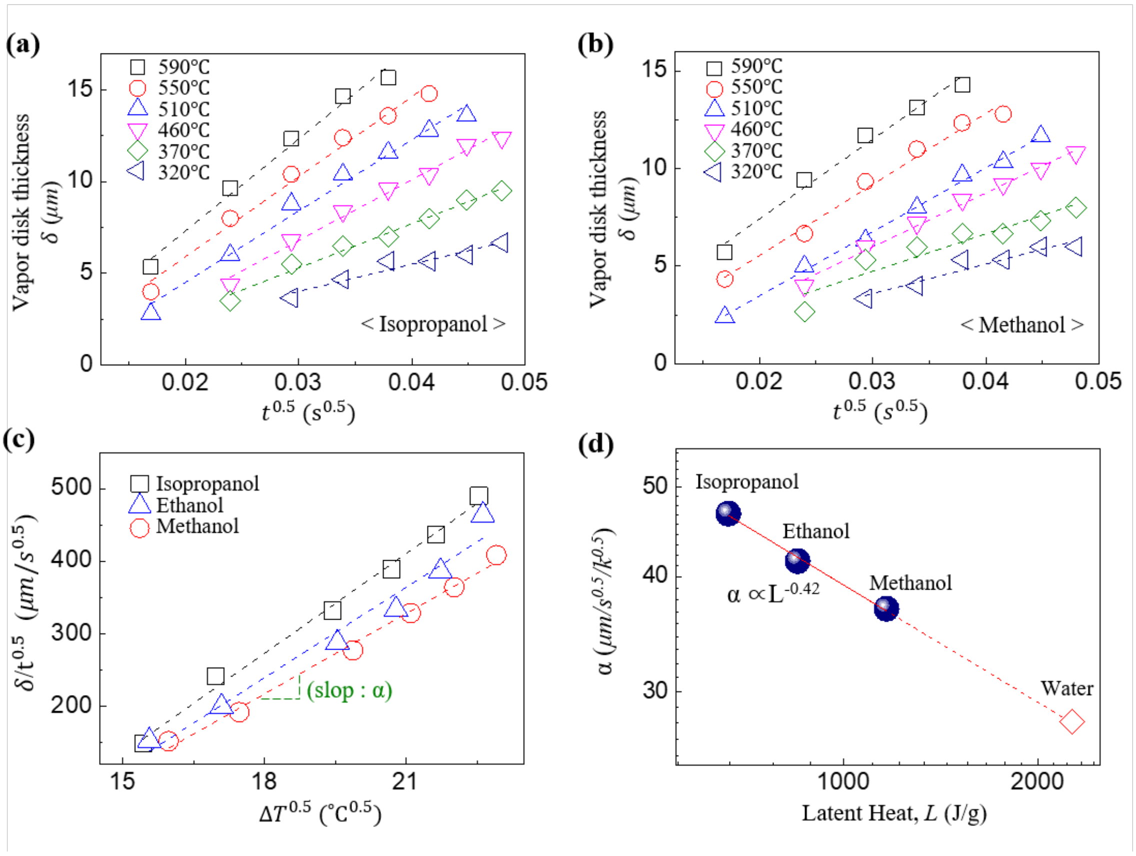

FIG. 8 (color online) Growth of vapor disks for various liquids. (a-b) Vapor disk thickness vs. $t^{0.5}$ in different T_s for **a** isopropanol and **b** methanol drops, consistently showing linear growth with $t^{0.5}$ regardless of temperature. Dashed lines are the best linear fittings of the data. The error bars are s.d. from the five to ten sets of image data. **(c)** Vapor disk thickness normalized by $t^{0.5}$ vs. $\Delta T^{0.5}$ for different liquids. α is the slope of $\delta/t^{0.5}$vs. $\Delta T^{0.5}$. **(d)** α vs. L (latent heat of the liquid drop); the red solid line is the best fit for the three liquids with allometric scaling : $\alpha \propto L^{-0.42}$. By extrapolating to water drop ($L \sim 2260$ J/g; red diamond), the α value for water is estimated as 2.9×10^{-5} $m/s^{0.5}/K^{0.5}$.